# Computer Simulations and Experiments on Vibration Control of a Flexible Link Manipulator Using a Piezoelectric Actuator

Abdul Kadir Muhammad, Barlas Raheel Khan, Shingo Okamoto, Jae Hoon Lee

***Abstract*— The purposes of this research are to formulate the equation of motion of the system, to develop computational codes by a finite-element method in order to perform dynamics simulation with vibration control, to propose an effective control scheme and to confirm the calculated results by experiments of a flexible link manipulator. The system used in this paper consists of an aluminum beam as a flexible link, a clamp-part, a servo motor to rotate the link and a piezoelectric actuator to control vibration. Computational codes on time history responses, FFT (Fast Fourier Transform) processing and eigenvalues - eigenvectors analysis were developed to calculate the dynamic behavior of the link. Furthermore, a control scheme using the piezoelectric actuator was designed to suppress the vibration. A proportional controller was designed and demonstrated its performances. The system and the proposed control scheme were confirmed through experiments. The calculated and experimental results revealed that the vibration of the flexible link manipulator can be controlled effectively.**

***Index Terms*—Finite element method, flexible manipulator, piezoelectric actuator, vibration control.**

## I. Introduction

EMPLOYMENT of flexible link manipulator is recommended in the industrial applications in order to accomplish high performance requirements such as high-speed and safe operation, increasing of positioning accuracy, less weight and lower energy consumption. However, a flexible link manipulator usually cannot be controlled easily because of its inheriting flexibility. Deformation of the flexible manipulator when it is operated must be considered in the control. Its controller system should deal with not only its motion but also vibration due to flexibility.

The purposes of this research are to formulate the equation of motion of the system, to develop computational codes by a finite-element method in order to perform dynamics simulation with vibration control, to propose an effective control scheme and to confirm the calculated results by experiment of the flexible link manipulator.

Manuscript received Jan 19, 2014; revised Feb 03, 2014.
Every author is with Mechanical Engineering Course, Graduate School of Science and Engineering, Ehime University, 3 Bunkyo-cho, Matsuyama 790-8577, Japan.
The first author is also with Center for Mechatronics and Control System, Mechanical Engineering Department, State Polytechnic of Ujung Pandang, Jl. Perintis Kemerdekaan KM 10 Makassar, 90-245, Indonesia.
Email: Shingo Okamoto <okamoto.shingo.mh@ehime-u.ac.jp>,
Jae Hoon Lee <jhlee@ehime-u.ac.jp>
Abdul Kadir Muhammad <y861008b@mails.cc.ehime-u.ac.jp>

The system used in this paper consists of an aluminum beam as a flexible link, a clamp-part, a servo motor to rotate the link and a piezoelectric actuator to suppress vibration. Computational codes on time history responses, FFT (Fast Fourier Transform) processing and eigenvalues - eigenvectors analysis were developed to calculate the dynamic behavior of the link validated by the experimental one.

Furthermore, a proportional (P) controller was designed to suppress the vibrations. It is done by adding moments of force generated by the piezoelectric actuator to the flexible link manipulator. Finally, the system and the proposed control scheme were confirmed trough experiments.

## II. Formulation by Finite Element Method

The link has been discretized by finite-elements. The finite-element has two degrees of freedom, namely the lateral deformation $v(t)$, and the rotational angle $\psi(t)$. The length, the cross-sectional area and the area moment of inertia around $z$-axis of every element are denoted by $l_i$, $S_i$ and $I_{zi}$ respectively. Mechanical properties of every element are denoted as Young's modulus $E_i$ and mass density $\rho_i$.

### A. Kinematic

Figure 1 shows the position vector of an arbitrary point P in the link in the global and rotating coordinate frames. Let the link as a flexible beam has a motion that is confined in the horizontal plane as shown in figure 1. The $O-XY$ frame is the global coordinate frame while $O-xy$ is the rotating coordinate frame fixed to the root of the link. A motor is installed on the root of the link. The rotational angle of the motor when the link rotates is denoted by $\theta(t)$.

The position vector $\boldsymbol{r}(x,t)$ of the arbitrary point $P$ in the link at time $t = t$, measured in the $O-XY$ frame shown in figure 1 is expressed by

$$\boldsymbol{r}(x,t) = X(x,t)\boldsymbol{I} + Y(x,t)\boldsymbol{J} \tag{1}$$

Where

$$X(x,t) = x\cos\theta(t) - v(t)\sin\theta(t) \tag{2}$$
$$Y(x,t) = x\sin\theta(t) + v(t)\cos\theta(t) \tag{3}$$

The velocity of $P$ is given by

$$\dot{\boldsymbol{r}}(x,t) = \dot{X}(x,t)\boldsymbol{I} + \dot{Y}(x,t)\boldsymbol{J} \tag{4}$$

ISBN: 978-988-19252-5-1
ISSN: 2078-0958 (Print); ISSN: 2078-0966 (Online)

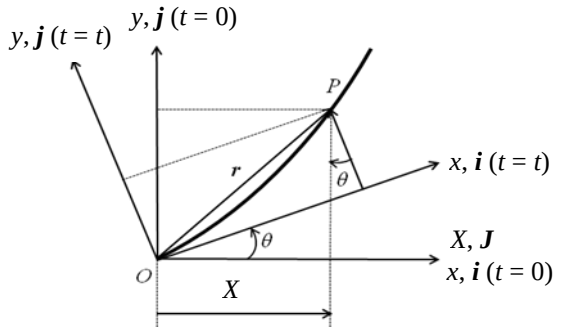


*O – XY*: Global coordinate frame
*O – xy* : Rotating coordinate frame

Fig. 1. Position vector of an arbitrary point *P* in the link in the global and rotating coordinate frames

### B. Finite Element Method

Figure 2 shows the rotating coordinate frame and the link divided by one-dimensional and two-node elements. Then, figure 3 shows the element coordinate frame of the *i-th* element. Here, there are four boundary conditions together at nodes *i* and (*i*+1) when the one-dimensional and two-node element is used. The four boundary conditions are expressed as nodal vector as follow

$$\boldsymbol{\delta}_i = \{v_i \quad \psi_i \quad v_{i+1} \quad \psi_{i+1}\}^T \tag{5}$$

Then, the hypothesized deformation has four constants as follows [1]

$$v_i = a_1 + a_2 x_i + a_3 {x_i}^2 + a_4 {x_i}^3 \tag{6}$$

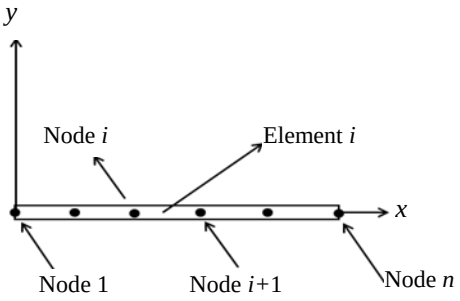


*o – xy*: Rotating coordinate frame

Fig. 2. Rotating coordinate frame and the link divided by the one-dimensional and two-node elements

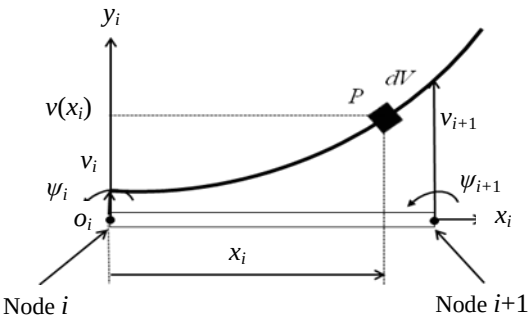


$o_i – x_i\, y_i$: Element coordinate frame of the *i*-th element

Fig. 3. Element coordinate frame of the *i-th* element

The relation between the lateral deformation $v_i$ and the rotational angle $\psi_i$ of the node *i* is given by

$$\psi_i = \frac{\partial v_i}{\partial x_i} \tag{7}$$

Furthermore, from mechanics of materials, the strain of node *i* can be defined by

$$\varepsilon_i = \varepsilon_{x_i} = -y_i \frac{\partial^2 v_i}{\partial {x_i}^2} \tag{8}$$

The experimental setup consists of mechanical structure of the flexible link manipulator, designed circuits and devices used to perform in this experiment.

### C. Equation of motion

Equation of motion of the *i-th* element is given by

$$\boldsymbol{M}_i \ddot{\boldsymbol{\delta}}_i + \boldsymbol{C}_i \dot{\boldsymbol{\delta}}_i + \left[\boldsymbol{K}_i - \dot{\theta}^2(t)\boldsymbol{M}_i\right]\boldsymbol{\delta}_i = \ddot{\theta}(t)\,\boldsymbol{f}_i \tag{9}$$

where $\boldsymbol{M}_i$, $\boldsymbol{C}_i$, $\boldsymbol{K}_i$, $\ddot{\theta}(t)\,\boldsymbol{f}_i$ are the mass matrix, damping matrix, stiffness matrix and the excitation force generated by the rotation of the motor respectively. The representation of the matrices and vector in Eq. (9) can be found in [2]. Finally, the equation of motion of the system with *n* elements considering the boundary conditions is given by

$$\boldsymbol{M}_n \ddot{\boldsymbol{\delta}}_n + \boldsymbol{C}_n \dot{\boldsymbol{\delta}}_n + \left[\boldsymbol{K}_n - \dot{\theta}^2(t)\boldsymbol{M}_n\ \boldsymbol{\delta}_n\right] = \ddot{\theta}(t)\,\boldsymbol{f}_n \tag{10}$$

## III. Validation of Formulation and Computational Codes

### A. Experimental Model

Figure 4 shows the experimental model of the flexible link manipulator. The flexible link manipulator consists of the flexible aluminum beam, the clamp-part, the servo motor and the base. The link is attached to the motor through the clamp-part. A strain gage is bonded to the position of 0.11 m from the origin of the link. The motor is mounted to the base. In the experiments, the motor was operated by an independent motion controller.

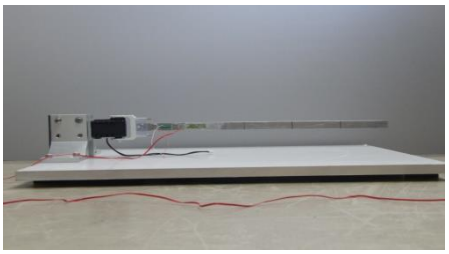

Fig. 4. Experimental model of the flexible link manipulator

### B. Computational Model

In this research, we defined and used two types of computational models of the flexible link manipulator.

ISBN: 978-988-19252-5-1
ISSN: 2078-0958 (Print); ISSN: 2078-0966 (Online)

*Model Ⅰ*

A model of only a flexible link manipulator was used as Model Ⅰ. Figure 5.a shows model Ⅰ. The link and the clamp-part were discretized by 5 elements and 1 element respectively. The clamp-part is much rigid than the link. Therefore Young's modulus of the clamp-part was set in 1,000 times of the link's. A strain gage is bonded to the position of Node 3 of the flexible link (0.11 m from the origin of the link).

*Model Ⅱ*

A model of the flexible link manipulator including the piezoelectric actuator was defined as Model Ⅱ. Figure 5.b shows model Ⅱ. The piezoelectric actuator was bonded to the one surface of element 2. The link was discretized by 22 elements. A schematic representation on modeling of the piezoelectric actuator is shown in figure 6. Physical parameters of the flexible link manipulator model and the piezoelectric actuator are shown in table 1.

The piezoelectric actuator suppressed the vibration of the flexible link manipulator by adding moments of force at nodes 2 and 3, $M_2$ and $M_3$ to the flexible link. The moments of force are generated by applying voltages $+E$ to the piezoelectric actuator as shown in figure 6. The relation between the moments of force and the voltages are related by

$$M_{2,3} = \pm d_1 E \tag{11}$$

Here $d_1$ is a constant quantity.

Furthermore, the voltage to generate the moments of force is proportional to the strain $\varepsilon$ of the single-link due to the vibration. The relation can be expressed as follows

$$E = \pm \frac{1}{d_2} \varepsilon \tag{12}$$

Here $d_2$ is a constant quantity. Then, $d_1$ and $d_2$ will be determined by comparing the calculated results and experimental ones.

Substituting Eq. (12) to Eq. (11) gives

$$M_{2,3} = \pm \frac{d_1}{d_2} \varepsilon \tag{13}$$

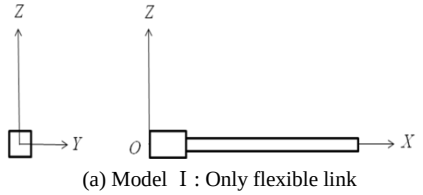


(a) Model Ⅰ: Only flexible link

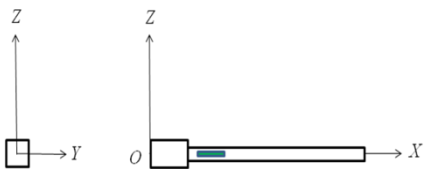


(b) Model Ⅱ: Flexible link with the actuator

Fig. 5. Computational models of the flexible link manipulator

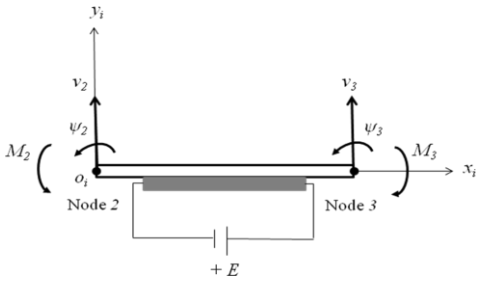


Fig. 6. Modeling of the piezoelectric actuator

TABLE I
PHYSICAL PARAMETERS OF THE FLEXIBLE LINK AND THE PIEZOELECTRIC ACTUATOR [2]

| | | |
|---|---|---|
| $l$ : Total length | m | $3.91 \times 10^{-1}$ |
| $l_l$ : Length of the link | m | $3.50 \times 10^{-1}$ |
| $l_c$ : Length of the clamp-part | m | $4.10 \times 10^{-2}$ |
| $l_a$ : Length of the actuator | m | $2.00 \times 10^{-2}$ |
| $S_l$ : Cross section area of the link | $m^2$ | $1.95 \times 10^{-5}$ |
| $S_c$ : Cross section area of the clamp-part | $m^2$ | $8.09 \times 10^{-4}$ |
| $S_a$ : Cross section area of the actuator | $m^2$ | $1.58 \times 10^{-5}$ |
| $I_{zl}$ : Cross section area moment of inertia around $z$-axis of the link | $m^4$ | $2.75 \times 10^{-12}$ |
| $I_{zc}$ : Cross section area moment of inertia around $z$-axis of the clamp-part | $m^4$ | $3.06 \times 10^{-8}$ |
| $I_{za}$ : Cross section area moment of inertia around $z$-axis of the actuator | $m^4$ | $1.61 \times 10^{-11}$ |
| $E_l$ : Young's Modulus of the link | GPa | $7.03 \times 10^{1}$ |
| $E_c$ : Young's Modulus of the clamp-part | GPa | $7.00 \times 10^{4}$ |
| $E_a$ : Young's Modulus of the actuator | GPa | $4.40 \times 10^{1}$ |
| $\rho_l$ : Density of the link | $kg/m^3$ | $2.68 \times 10^{3}$ |
| $\rho_c$ : Density of the clamp-part | $kg/m^3$ | $9.50 \times 10^{2}$ |
| $\rho_a$ : Density of the actuator | $kg/m^3$ | $3.33 \times 10^{3}$ |
| $\alpha$ : Damping factor of the link | - | $2.50 \times 10^{-4}$ |

*C. Time History Responses of Free Vibration*

Experiment on free vibration was conducted using an impulse force as an external one. Figure 7 shows the experimental time history response of strains $\varepsilon_e$ on the free vibration at the same position in the calculation.

Furthermore, the computational codes on time history response of Model Ⅰ were developed. Figure 8 shows the calculated strains at Node 3 of Model Ⅰ under the impulse force.

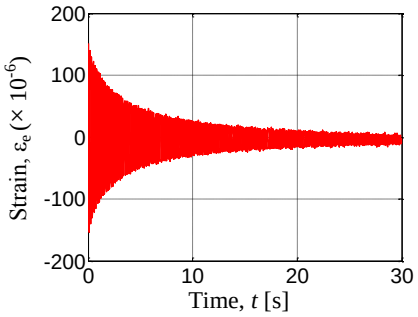


Fig. 7. Experimental time history response of strains on free vibration of the flexible link at 0.11 m from the origin of the link

ISBN: 978-988-19252-5-1
ISSN: 2078-0958 (Print); ISSN: 2078-0966 (Online)

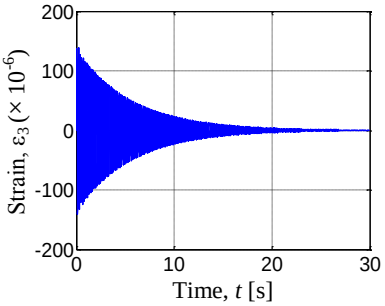


Fig. 8. Calculated time history response of strains on free vibration at Node 3 of Model I

### D. Fast Fourier Transform (FFT) Processing

Both the experimental and calculated time history responses of free vibration of Model I were transferred by FFT processing to find their frequencies.

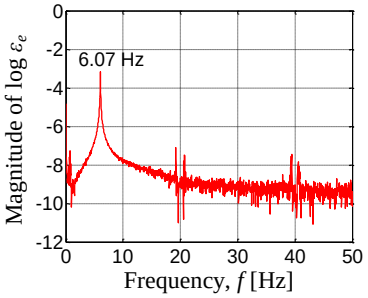


Fig. 9. Experimental natural frequencies of the flexible link

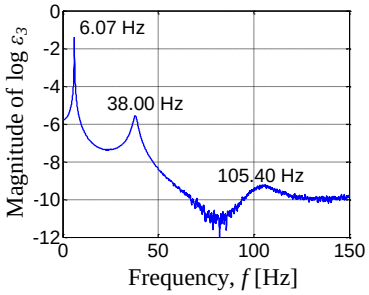


Fig. 10. Calculated natural frequencies of Model I

Figures 9 and 10 show the experimental and calculated natural frequencies of the flexible link manipulator, respectively. The experimental first natural frequency, 6.07 Hz well agreed with the calculated one. The second and third experimental natural frequencies could not be measured. However, in the calculation, they could be obtained as 38.00 Hz and 105.40 Hz.

### E. Eigen-values and Eigen-vectors Analysis

The computational codes on Eigen-values and Eigen-vectors analysis were developed for natural frequencies and vibration modes.

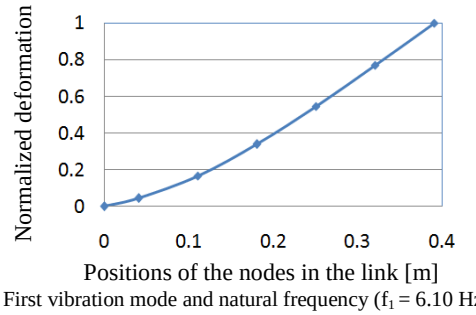


Fig. 11. First vibration mode and natural frequency ($f_1$ = 6.10 Hz) of Model I

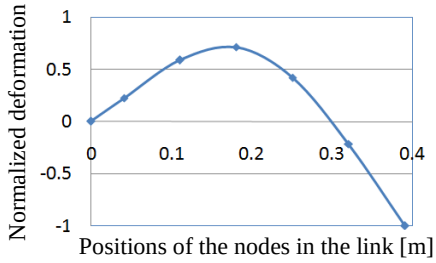


(a) Second vibration mode and natural frequency ($f_2$ = 38.22 Hz)

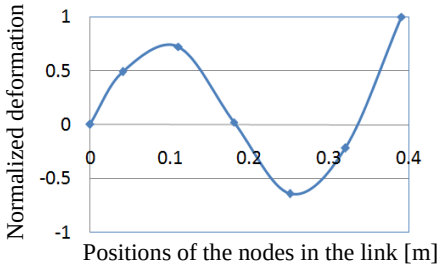


(b) Third vibration mode and natural frequency ($f_3$ = 107.19 Hz)

Fig. 12. Vibration modes and natural frequencies of Model I

The calculated results for the first, second and third natural frequencies were 6.10 Hz, 38.22 Hz, and 107.19 Hz respectively. The vibration modes of natural frequencies are shown in figure 11, 12.a and 12.b.

### F. Time History Responses due to the Excitation Force

Another experiment was conducted to investigate the vibration of the flexible link due to the excitation force generated by rotation of the motor. In the experiment, the motor was rotated by the angle of $\pi/2$ radians (90 degrees) for 2.05 seconds. Figure 13 shows the experimental time history response of strains of the flexible link due to the motor's rotation at 0.11 m from the origin of the link. Based on figure 13, the angular acceleration of the motor was calculated. Time history response of the motor's acceleration is shown in figure 14. Furthermore, based on figures 11 and 12, the time history response of strains at Node 3 of Model I was calculated as shown in figure 15.

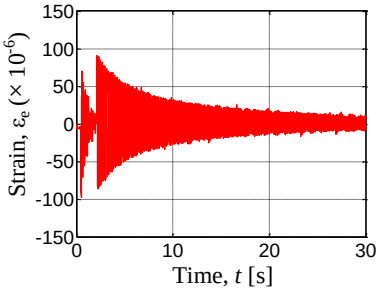


Fig. 13. Experimental time history responses of strains at 0.11 m from the origin of the link

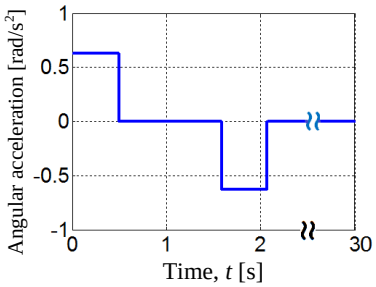


Fig. 14. Time history response of angular acceleration of the motor

ISBN: 978-988-19252-5-1
ISSN: 2078-0958 (Print); ISSN: 2078-0966 (Online)

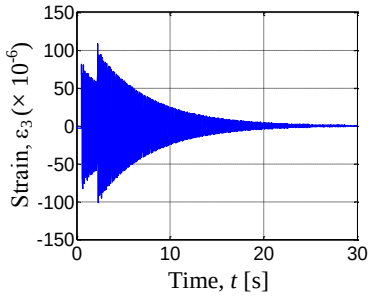


Fig. 15. Calculated time history responses of strains at Node 3 of Model I due to the excitation force generated by the motor's rotation

The above results show the validities of the formulation, computational codes and modeling the flexible link manipulator.

## IV. Control Scheme

As one of the conclusions of the previous work, a proportional controller is sufficient for practical applications of the system [2]. Therefore, a proportional controller, $K_p$ was designed so that vibration due to motor's rotation of the flexible link system can become smaller.

Based on equation (13), the control force can be defined by a vector as follows

$$\boldsymbol{u}_n(t) = \{0 \quad 0 \quad 0 \quad K_p \quad 0 \quad -K_p \quad 0 \quad \cdots \quad 0\}^T(\varepsilon_d - \varepsilon_3) \tag{14}$$

where $\varepsilon_d$ and $\varepsilon_3$ denote the desired and measured strains at Node 3, respectively. The gain of P-controller by the actuator can be written by a vector in *s*-domain as follows

$$\boldsymbol{G}_C(s) = \{0 \quad 0 \quad 0 \quad K_p \quad 0 \quad -K_p \quad 0 \quad \cdots \quad 0\}^T \tag{15}$$

Furthermore, the equation of motion of the controlled flexible link manipulator with *n* elements is given by

$$\boldsymbol{M}_n\ddot{\boldsymbol{\delta}}_n + \boldsymbol{C}_n\dot{\boldsymbol{\delta}}_n + \left[\boldsymbol{K}_n - \dot{\theta}^2(t)\boldsymbol{M}_n\right]\boldsymbol{\delta}_n = \ddot{\theta}(t)\boldsymbol{f}_n + \boldsymbol{u}_n(t) \tag{16}$$

Finally, block diagram of feedback control of the flexible link is shown in figure 16.

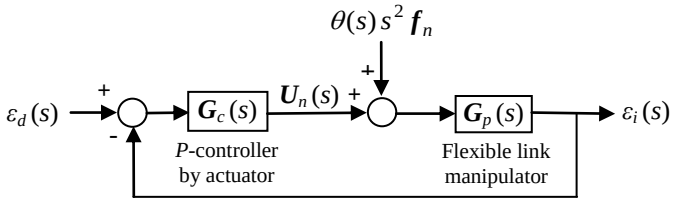


$\varepsilon_d$ : Desired strain, $\varepsilon_i$ : Measured strains at Node *i*

Fig. 16. Block diagram of feedback control of the flexible link manipulator

## V. Experiment

### A. Experimental Set-up

In order to investigate the validity of the proposed control scheme, an experimental set-up was designed. The set-up is shown in Fig.17. The flexible link manipulator consists of the flexible aluminum beam, the clamp-part, the servo motor and the base. The flexible link was attached to the motor through the clamp-part. In the experiments, the motor was operated by an independent motion controller. A strain gage was bonded to the position of 0.11 m from the origin of the link.

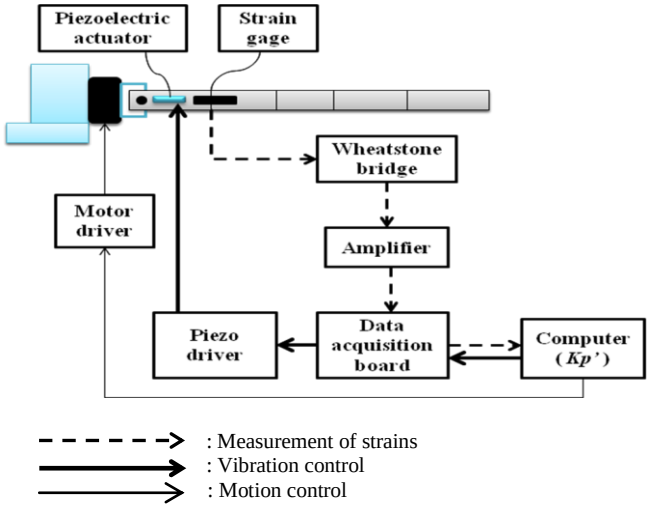


Fig. 17. Schematics of measurement and control system

The piezoelectric actuator was attached on one side of the flexible robotic arm to provide the blocking force against vibrations. A Wheatstone bridge circuit was developed to measure the change in resistance of the strain gage sensor in the form of voltage. An amplifier circuit was designed to amplify the small output signal of the Wheatstone bridge. A data acquisition board and a computer that have functionality of A/D (analog to digital) conversion, signal processing, control process and D/A (digital to analog) conversion were used. The data acquisition board connected to the computer through USB port. Finally, the controlled signals sent to a piezo driver to drive the piezoelectric actuator in its voltage range.

### B. Experimental Method

The rotation of the motor was set from 0 to $\pi/2$ radians (90 degrees). The outputs of strain gage were converted to voltages by the Wheatstone bridge and magnified by the amplifier. The noises that occur in the experiment were reduced by a 3.3 [μF] capacitor attached to the amplifier. The output voltages of the amplifier sent to the data acquisition board and the computer for control process. The proportional control scheme was implemented in the computer using the visual C++ program. The analog output voltages of the data acquisition board sent to the input channel of the piezo driver to generate the actuated signals for the piezoelectric actuator.

## VI. Calculated and Experimental Results

### A. Calculated Results

Time history responses of strains on the controlled system were calculated for Model II under the control scheme as shown in figure 14. They were calculated when the motor rotated by the angle of $\pi/2$ radians (90 degrees). Control algorithms were design so that control force of the actuator can suppress vibration on one side and both sides of the flexible link. Examining several gains of the proportional controller leaded to $K_p$ = 600 [Nm] as the better one. Figure 18(a) shows the uncontrolled and controlled time history responses of strains at Node 3 for the one-side control. The maximum strain of uncontrolled system became $-92.40\times10^{-6}$ and the controlled one became $23.70\times10^{-6}$, as shown in figure 18(a). Figure 18(b) shows the uncontrolled and controlled time history responses of strains at Node 3 for the both-sides control. The maximum strain of controlled system became $33.50\times10^{-6}$, as shown in figure 18(b).

ISBN: 978-988-19252-5-1
ISSN: 2078-0958 (Print); ISSN: 2078-0966 (Online)

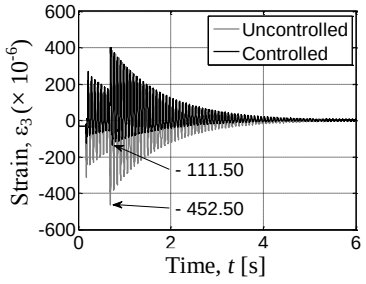


(a) $K_p$ = 600 [Nm] applied for one-side control

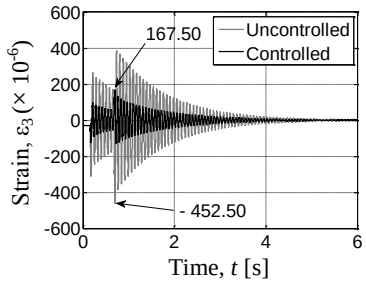


(b) $K_p$ = 600 [Nm] applied for both-sides control

Fig. 18. Calculated time history response of strains at Node 3 for uncontrolled and controlled Model Ⅱ due to the excitation force of the motor's rotation

### B. *Experimental Results*

Experimental time history responses of strains on the controlled system were measured under the control scheme as shown in figure 17. The strains were measured when the motor rotated by the angle of $\pi/2$ radians (90 degrees).

Firstly, based on the proportional gain used in the calculation, an experimental P-gain that is non-dimensional gain, $K_p'$ = 600 was applied to the system. Secondly, the gain was tuned until $K_p'$ = 800 for one-side control and until $K_p'$ = 1,000 for both-sides control to find the better response. Figures 19 and 20 show the uncontrolled and controlled experimental time history responses of strains at the same position in the calculation using $K_p'$ = 600 and $K_p'$ = 800 for the one-side control. The maximum strain of uncontrolled system was $-448.50\times10^{-6}$ and the controlled one became $-327.00\times10^{-6}$ using $K_p'$ = 600, as shown in figure 19. The maximum strain of controlled system using $K_p'$ = 800 becomes $-241.00\times10^{-6}$, as shown in figure 20. Furthermore, figures 21(a) and 21(b) show the uncontrolled and controlled experimental results of strains at the same position as the calculation using $K_p'$ = 600 and $K_p'$ = 1,000 for the both-sides control. The maximum strain of controlled system became $-348.80\times10^{-6}$ using $K_p'$ = 600, as shown in figure 21(a) The maximum strain of controlled system using $K_p'$ = 1,000 became $-272.70\times10^{-6}$, as shown in figure 21(b)

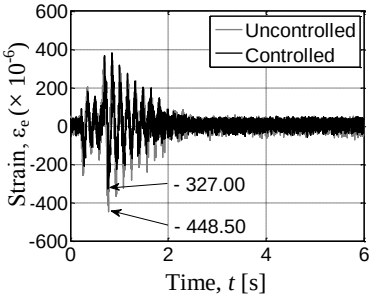


Fig. 19. Experimental time history responses of strains at 0.11 m from the link's origin for uncontrolled and controlled system due to the excitation force of the motor's rotation ($K_p'$ = 600 applied for one-side control)

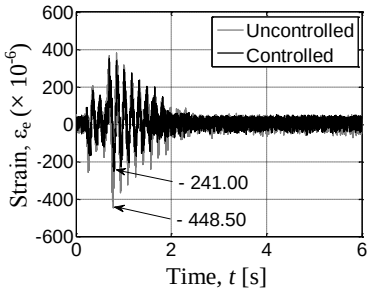


Fig. 20. Experimental time history responses of strains at 0.11 m from the link's origin for uncontrolled and controlled system due to the excitation force of the motor's rotation ($K_p'$ = 800 applied for one-side control)

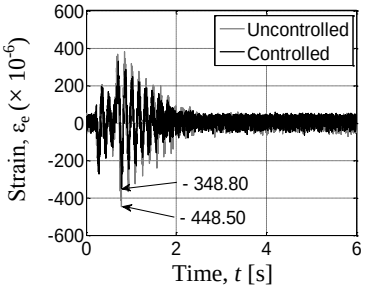


(a) $K_p'$ = 600 applied for both-sides control

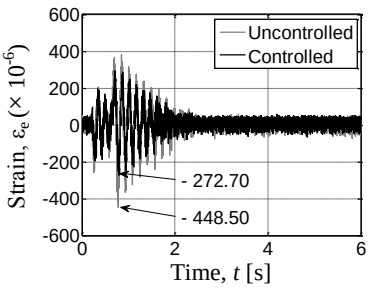


(b) $K_p'$ = 1,000 applied for both-sides control

Fig. 21. Experimental time history responses of strains at 0.11 m from the link's origin for uncontrolled and controlled system due to the excitation force of the motor's rotation

These results verify that the proposed control scheme can effectively suppress the vibration of the flexible link manipulator.

## VII. Conclusion

The equation of motion for the flexible link manipulator had been derived using the finite-element method. Computational codes had been developed in order to perform dynamic simulations of the system. Experimental and calculated results on time history responses, natural frequencies and vibration modes show the validities of the formulation, computational codes and modeling of the system. A simple and effective control scheme was designed to suppress the vibration of the system. The proposed control scheme was examined through the calculations and experiments. The calculated and experimental results have been revealed that the vibration of the flexible link manipulator can be suppressed effectively.

## References

[1] M. Lalanne, P. Berthier, J. D. Hagopiean , *Mechanical Vibration for Engineers*, John Wiley & Sons Ltd, 1983, pp. 146 -153.

[2] A.K. Muhammad, S. Okamoto and J.H. Lee, "Computer Simulations on Vibration Control of a Flexible Single-link Manipulator Using Finite-element Method", in *Proc. 19th Annu. Int. Conf. Artificial Live and Robotics*, Japan, 2014.

[3] www.mmech.com, *Resin Coated Multilayer Piezoelectric Actuators.*